Experimental Investigation of Tidal Rotor Loading due to Wave, Current and Impact with Sea Animals

Experimental Investigation of Tidal Rotor Loading due to Wave, Current and Impact with Sea Animals

Grégory S. Payne*†,Tim Stallard†† and Rodrigo Martinez*‡

*Institute for Energy Systems, The University of Edinburgh
Edinburgh, United Kingdom
†E-mail: gregory.payne@ed.ac.uk
‡E-mail: r.martinez@ed.ac.uk

††School of Mechanical Aerospace and Civil Engineering
The University of Manchester
Manchester, United Kingdom
E-mail: tim.stallard@manchester.ac.uk

***Abstract*—Extreme loading and associated survivability are key aspects of tidal turbines. This study focuses on the experimental investigation of extreme loads due to combined wave and current hydrodynamic loading and impact loads arising from collision with large sea animals. The design process and commissioning for reduced scale experiments to quantify such loads is described and preliminary findings are presented. The tidal device considered is a generic three bladed horizontal axis turbine. The scale of the model is approximately 1/15 relative to a typical full-scale turbine. The rotor is designed so that the thrust and power coefficient as a function of tip speed ratio represent a full-scale prototype and prior experiments. Blade design was carried out by combining an in-house blade element momentum code with a finite element analysis. Impact loads were estimated using a separate experimental apparatus consisting of a rotating arm, with similar inertia to that of the rotor, which hits a target with similar mechanical properties to those of a marine animal. Preliminary analysis indicates that impact loads are higher than hydrodynamic loads, by a factor of more than fifty for impact with a hard object. Impact with a deformable object, representing blubber of a marine, are lower but indicate negligible dependence on object mass and are greater than the predicted hydrodynamic loads. Experimental results from this campaign of tests will serve as benchmark data to validate computational fluid dynamics (CFD) of hydrodynamic loading and smooth particle hydrodynamic lattice spring modelling (SPH-LSM) of impact loading.**

***Index Terms*—tidal turbine, experiment, extreme loads, wave and current, impact loads**

I. Introduction

Tidal energy has seen a rapid development over recent years with several developers now conducting offshore trials of full-scale prototypes generating electricity to a grid. These machines are pre-commercial (Technology Readiness Level (TRL) 8) and it is expected that further technological development will reduce cost towards the range required for TRL 9. For design it is important to predict the occurrence and magnitude of loading over the design life of a turbine and its sub-components.

Loading is influenced by the environmental conditions such as mean velocity and turbulence intensity of the flow and significant wave height and period of surface waves. Loading is also influenced by the turbine operating point with load shedding, such as by pitch control, typically implemented above rated speed. Understanding the peak load associated with typical operating conditions is therefore important. There have been various studies of the influence of ambient turbulence and wake turbulence on mean loading including by engineering design tools [1], [2], experimental analysis [3], [4] and CFD simulation [5]. Wave induced loads have also been studied by experiments in towing tanks [6], [7] and in steady flow [8], [9] and reasonable agreement has been observed with blade element predictions. However, there remains limited understanding of load variation due to following, opposing or oblique waves and there has been limited evaluation of CFD for this purpose.

Tidal stream turbines may also be subject to loading due to impact from floating bodies such as containers, flotsam, and potentially from marine vertebrates such as seals and whales [10]. There is uncertainty concerning both the likelihood and severity of impact between blade, or turbine, and floating debris which may be immersed due to breaking waves or due to buoyancy. Impact may thus be with bodies of a range of sizes and mechanical properties [10], [11]. This study focuses on experimental investigation of peak loading due to combination of turbulent current and waves and on impact loads arising from collision with large sea animals. The paper provides an overview of the design process for a turbine model to study these loads and preliminary findings are presented.

The tidal device considered is a generic three bladed horizontal axis turbine with diameter 1.2m. The trajectory of a floating body through a rotor plane will depend on the velocity field from upstream of the rotor to the rotor

plane. The rotor geometry and experimental arrangement was thus selected to facilitate comparison to prior and ongoing experimental and numerical investigations for which wake characteristics and load data are available. Radial variation of chord length and pitch were selected to develop thrust variation representative of a generic full-scale turbine [12]. A depth of 1.67 times the diameter was considered, for which experimental measurements are available of the mean velocity-field [13] and of the variation of loading due to turbulence and opposing waves [9]. This data was for approximately 1:70 scale based on turbine diameter whereas the present study concerns approximately 1:15 scale. Numerical simulations of the loading of a generic full-scale turbine used as the basis of design are also available [14] and experiments reported by [3] exhibit a comparable thrust curve to the turbine considered. Data from the present series of experiments will inform the evaluation of a CFD method to assess the relative magnitude of unsteady loads due to waves, velocity shear [15] and turbulence [5].

An investigation of impact loads is given in section II to inform blade design. The approach to selection of blade profile and blade structural design is detailed in section III. Section IV details the design of drivetrain and both shaft and blade instrumentation based on the established load ranges. A summary of the design is given in section V and findings of an ongoing experimental programme will be presented at the conference.

II. Preliminary Impact Tests

It was originally considered that a single physical turbine model would be used to investigate both hydrodynamic extreme loads (due to turbulence and waves) and impact loads associated with collision with sea animals. There were subsequent concerns that forces induced by impact tests would be significantly larger than those associated with hydrodynamic loads and that it might therefore not be realistic to design a single model with instrumentation sufficiently robust to withstand and measure impact loads whilst also sensitive enough to measure hydrodynamics loads. It was therefore decided to carry out preliminary impact tests with a simplified experimental set-up.

The scaling of physical impact tests is complex and it is not intended for these preliminary impact measurements at small scale to be extrapolated to full scale. Instead, the intention is to provide impact force measurements on a variety of materials which have similar mechanical properties to the skin, bones and flesh of sea animals [10], [11] both to assess dependence on the characteristics of the impacted object and for use for evaluation of numerical models of these kind of impacts [16]. Moreover these measurements are useful to inform the design of the turbine model.

A. Experimental apparatus

To reduce the level of complexity associated with these preliminary impact tests, they were carried out in the dry with a stationary target. This approach neglects the possible reduction of impact velocity due to induced velocity of the target and the hydrodynamic added mass and damping of the body so the loading may only be considered indicative. However, this was considered sufficient as a first step to identifying the relevant load range for design. Figure 1 shows the experimental apparatus.

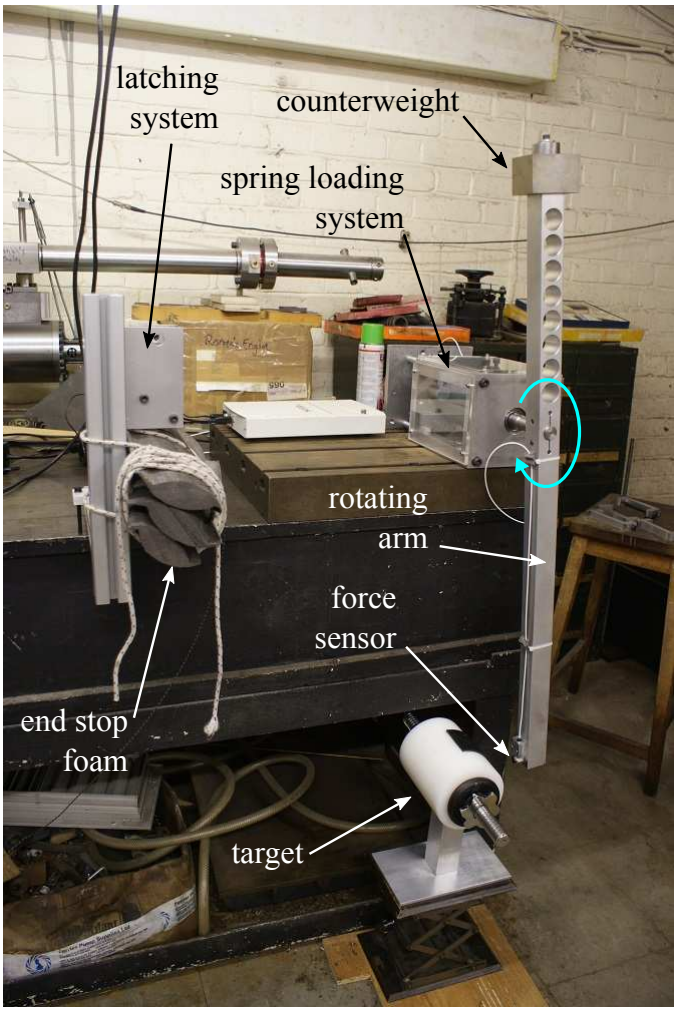

Fig. 1. Impact load test rig. The blue arrow shows the rotation movement of the arm when driven by the spring

A single turbine blade was simulated by a single robust rotating arm whose radius was that of the rotor (0.6m). The arm was designed so that its moment of inertia about its rotating axis is equal to that of the turbine rotor plus added inertia. The latter was estimated using strip theory and assuming that the two-dimensional added mass of the local blade section is that of an ellipse whose minor axis is equal to the local blade thickness and the major axis is equal to the local chord length. The two-dimensional

calculations of the added mass of each ellipse assumes steady state and is based on potential flow theory [17]. One of the sides of the arm was shorter than the other so that only one side was long enough to hit the target. To keep the arm balanced about its rotation axis, holes were drilled on the shorter side and a counterweight affixed to the tip. The arm is made of aluminium alloy and the counterweight of steel. The theoretical moment of inertia of the arm was computed at design stage using a CAD software but its actual value, accounting for all the rotating parts, including shaft and fittings was measured experimentally using a torsional pendulum and found to be 0.5239kgm^2.

The rotational speed of the arm is measured using a brushed printed armature motor used as a tachogenerator. The rig was initially fitted with a digital encoder but vibrations induced by the impact through the whole system created a large amount of jitter with the encoder, rendering its output unusable. The tachogenerator is mounted in-line with the shaft of the system and was calibrated using a lathe. Forces at impact are measured using piezoelectric force sensor. Piezoelectric technology was preferred over stain gauge based transducers as it is more robust, stiffer and well suited to measure short impulsive loads. The model used for the rig is a 208C05 made by the company PCB Piezotronics. Voltage signals from both instruments were recorded using a National Instruments data acquisition system (USB-6229).

The rotating arm is driven by a custom made torsion spring. The spring was wound by 160° prior to release. This was achieved by rotating the arm by hand in the opposite direction to that shown by the blue arrow in figure 1. The arm was then locked using a latching mechanism which was released remotely. Following release the arm accelerated over the first 180° and for the last 90°, the system free-wheels until impact on the target. The spring has several pre-loading settings which were preset to develop pre-impact rotational speeds ranging from 35 and 110 r/min.

The target consists of a high-density polyethylene (HDPE) plastic cylinder covered at the point of impact with a 3mm natural rubber sheet. The cylinder has a 20mm diameter hole through its axis through which a steel bar can be fitted. Weight discs can be mounted onto the bar to modify the mass of the target. Prior to impact the target rests on a stand in the manner of a golf ball on a tee.

The test rig was bolted onto a large cast iron table whose mass is estimated to be over one tonne. This ensured that the experimental rig had a stable position when impacts took place and that the impact forces measured could be measured accurately.

B. Impact tests results

Impact tests were carried out with four configurations of target:

- 1.6kg mass with impact taking place on the rubber sheet
- 4.4kg mass with impact taking place on the rubber sheet
- 1.6kg mass with impact taking place directly on the harder HDPE plastic
- 4.4kg mass with impact taking place directly on the harder HDPE plastic

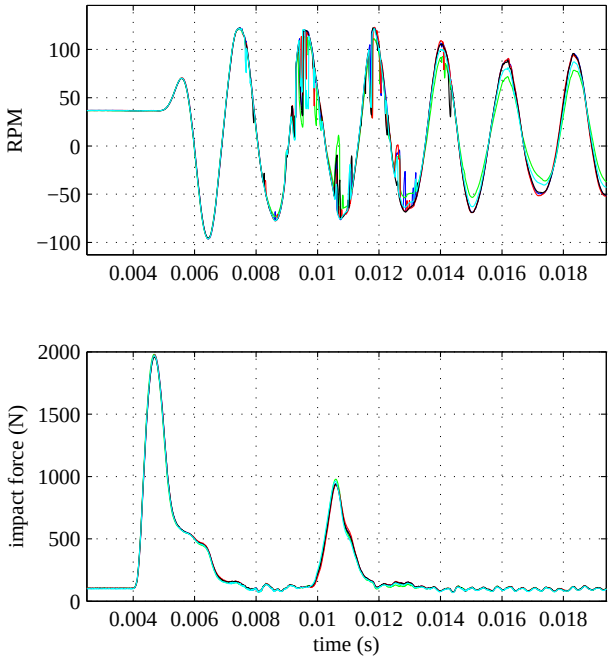

Fig. 2. Time series of the arm rotational velocity (top) and impact force (bottom) for the impact with a 1.6kg target on the rubber sheet with pre-impact velocity of 37 r/min. The five traces of different colours correspond to five repetition of the experiment.

Figure 2 shows the time series of the arm rotational speed (top graph) and of the impact force (bottom graph). Both plots share the same time line. These graphs correspond to impacts on the 1.6kg target fitted with the rubber sheet. The pre-impact rotational velocity of the arm is 37 r/min which corresponds to a tip speed ratio (TSR) of 2.3 for a 1ms^{-1} free stream velocity. Each graph contains five traces corresponding to five repetitions of the same experiment.

The first thing that can be noticed from figure 2 is that the repeatability is excellent. On the impact force plot, the five lines are almost indistinguishable. From the moment of the impact, the impact force trace shoots to a peak of just under 2000N within 0.5ms. It is interesting to notice that the maximum value of the impact force is reached before the velocity trace is significantly affected. This is believed to be due to the fact that on impact, the arm first deforms before the velocity variations are passed on to the shaft and hence to the tachogenerator. The secondary impact force peaks are believed to be due to structural vibrations of the arm induced by the impact. On impact, the arm will bend

away from the target and thus starting structural oscillations. As the arm bends away, the tip velocity component induced by the structural oscillations is in the opposite direction to the component of the tip velocity which is due to the overall arm rotary motion. The target is also accelerated by the impact force. The relative velocity between the tip and the target therefore goes down. At that stage, the tip and the target are still in contact and that reduction in relative velocity leads to a decrease in impact force after the first peak. When the tip of the arm has reached its maximum deflection, the tip velocity component induced by vibration is zero and the relative velocity between the tip and the target therefore decreases less. This is believed to correspond to the inflection of the impact force curve at 5.2ms. Shortly after that, the relative velocity between the tip and the target is close to zero (between 7 and 10ms), hence the low impact force during that period. There is then a significant secondary peak which is believed to be due to the the tip velocity component induced vibration being maximum and in the same direction as velocity due to the rotary arm motion.

Looking at the rotational speed trace, it can be seen that shortly after impact, the RPM trace oscillates at a constant frequency close to 500Hz. This frequency corresponds to the natural frequency of the overall system (arm + shaft + tachogenerator). This was confirmed by subjecting the test rig to an impulse excitation (by gently hitting it with a hammer) and looking at the tachogenerator signal. Regardless of the location at which the test rig is hit, the frequency of the signal oscillations remains close to 500Hz. When the arm impacts the target, this generate a large impulse excitation and the system then vibrates at its natural frequency.

The RPM time series also exhibits some jitter shortly after the velocity starts to oscillate. These get more pronounced as the amplitude of the RPM oscillations increase and gradually dwindle as the oscillations amplitude decreases. The frequency of those jitters is more than an order of magnitude higher than the natural mechanical frequency of the test-rig. The shape of the jitter pulsation is not sinusoidal. Moreover the jitter trace seems to go vertically from the 'undisturbed' sinusoidal signal pattern towards zero RPM but rarely crossing that zero RPM line, regardless whether the 'undisturbed' sinusoidal signal pattern is positive or negative. For a tachogenerator, a zero RPM reading corresponds to a zero voltage signal. All these elements tend to point to the fact that these jitters are not due to a purely mechanical phenomenon but rather to an electrical one. It could have something to do with the fact that the motor, used as a tachogenerator, is brushed and that some of the vibrations generated by the impact affect the contact between the brushes and the shaft commutator.

Impact tests were carried out with the four target configurations described earlier and for pre-impact rotational velocities ranging from 36 to 105 r/min (corresponding to a TSR range of 2.3 to 6.6 in 1ms^{-1} free stream velocity current). Each individual test was repeated five times. The outcome of these tests are summarised by figure 3 which plots the maximum impact load value (i.e. the value of the first impact force peak) against pre-impact rotational speed. Each point on the graph corresponds to the mean of the five test repetitions. The error bars correspond the standard deviation in velocity and impact force. From figure 3 it can be seen that the two main factors affecting the maximum impact force are the material of the target at the point of impact and the pre-impact velocity. The mass of the target has little bearing on the impact force value. The impact force directly on the plastic is more than double that of when the plastic is covered by a 3mm sheet of natural rubber. This applies across the full range of impact velocities studied and it is evident that the maximum impact force increases linearly with pre-impact velocity.

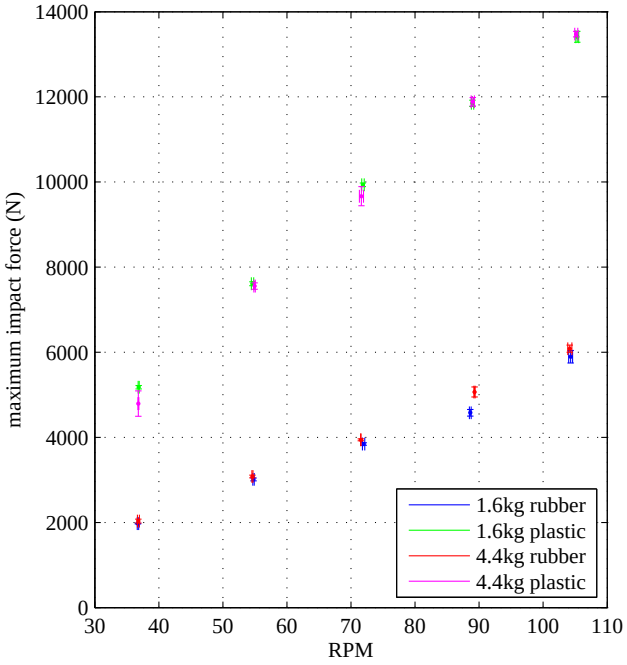

Fig. 3. Maximum impact force versus pre-impact rotational speed for two target masses and two target material at the point of impact. Each point is derived from the mean of five test repetitions and the error bars correspond to standard deviation

Preliminary impact tests have also been carried out with a softer target more representative of blubber [10], [11]. That target is shown in figure 4. The target comprises a cylinder 110mm in diameter and 200mm long. Its structure consists of two plastic discs (white on figure 4), one at each end of the cylinder, connected together in their middle with a 12.7mm diameter aluminium alloy rod. A tube of soft 3mm thick natural rubber spreads from one disc to the other (brown on figure 4). The target is filled with ballistic gel made from 300 Bloom gelatine powder supplied by MM Ingredients Ltd. The mass of the target is 1.99kg.

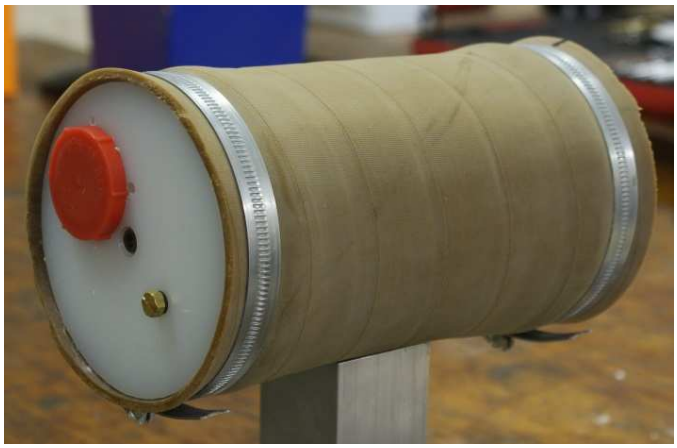

Fig. 4. Soft target

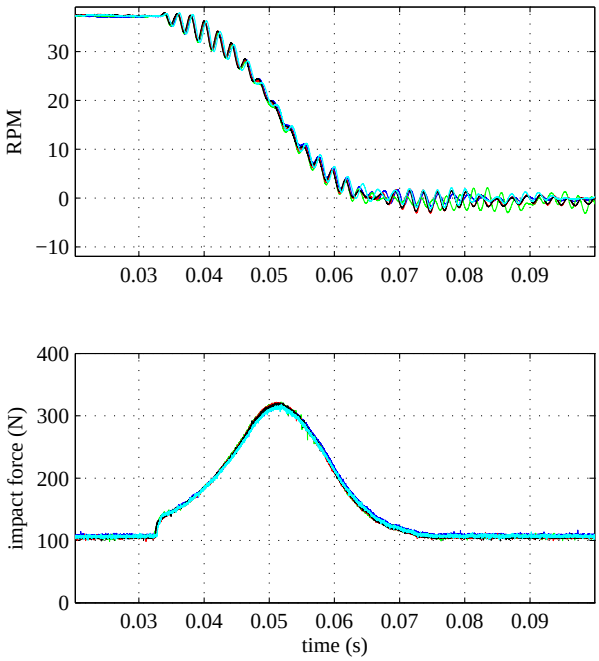

Fig. 5. Time series of the arm rotational velocity (top) and impact force (bottom) for the impact with a 1.6kg 'soft' target with pre-impact velocity of 37 r/min. The five traces of different colours correspond to five repetition of the experiment.

Figure 5 shows the time series of rotational velocity and impact force for the 'soft' target with a pre-impact speed of 37r/min. As with the harder target, the repeatability is excellent. Compared with the impact of figure 2, the maximum impact force is almost an order of magnitude lower but the peak spreads over a longer duration (40 instead of 1.3ms). The vibrations observed on the speed time series have the same frequency but are much less severe. All this makes sense given the softer nature of the target. It is also interesting to notice that impact on the 'soft' target does not lead to multiple force peaks. Further tests at higher speed should be carried out with the 'soft' target to investigate how maximum impact force evolves with speed.

These preliminary impact tests provide useful informations for the design of the turbine model. Although impact on the 'soft' target are associated with reasonably low forces (just over 300N), impact forces on the HDPE target covered with a sheet of rubber can be more than an order of magnitude higher (6000N). The latter corresponds to a worst case scenario where the tip of the turbine model blade would hit a 'hard part' of the sea animal model. This may represent an extreme case which would both a turbine model and its instrumentation would need to withstand and measure.

III. Rotor Design

A high stiffness blade design has been developed based on the peak hydrodynamic load in the streamwise and azimuthal directions. High stiffness was selected to minimise tip deflection (to within 2% of radius) and thus allow representation of the wetted geometry with a non-deforming CFD mesh. Blades were designed based on radial variation of blade loads assuming quasi-steady flow. Loads were analysed for constant speed operation to facilitate CFD simulation of the fixed pitch turbine load variation due to turbulent flow with waves. Radial variation of blade loads were used as input to a structural model of the blade to assess deflection and possible failure. The design was iterated to facilitate manufacture.

A. Hydrodynamic Loads

To initially model the hydrodynamic forces applied to the rotor, a standard, in-house, blade element momentum (BEM) code has been employed. The theory and equations on which this code is based can be found in [18] and this has demonstrated reasonable agreement with mean loading of a reduced scale turbine [9]. The BEM model provides a radial distribution of streamwise and off-axis (perpendicular to the streamwise direction) loads applied on each blade for a specified (steady) onset velocity and constant rotational speed.

For design, peak and mean loads are considered. These were estimated assuming superposition of a mean flow speed of 1ms^{-1} and the maximum expected wave induced velocity. It is assumed that the largest sea-state to which the full scale turbine is exposed to is characterised by $H_{m_0} = 3$m. The average of the hundredth highest waves is then taken as the largest wave the turbine will experience. Under the assumption of a Rayleigh distribution, this is given by $H_{1/100} = 1.66 H_{m_0}$ [19]. The wave period of this large wave is assumed to be 10s. Based on Froude scaling, at model scale, the corresponding 'extreme' regular wave has an amplitude of 0.166m and a period of 2.58s. The amplitude of the horizontal component of the wave induced water particle velocity was given by linear wave theory. Integration of the

velocity over the rotor plane for a regular wave of amplitude $a = 0.166$m and a period of $T = 2.58$s yields a mean horizontal wave induced water particle velocity of 0.28ms^{-1}. Design loads were thus estimated for a quasi-steady flows in the range 0.72 to 1.28ms^{-1}.

The rotor was designed to represent variation of thrust coefficient, C_T at tip speed ratio representative of operation of a generic full-scale turbine. A similar approach to turbine design has previously been used to develop rotors for experimental studies of turbine wakes [13] and CFD simulations of effect of shear on loading [14]. For these rotors there is only small variation of thrust coefficient over the tip speed ratio range 4-7 which facilitates analysis of the influence of onset flow variation on load variation. Similar thrust curves are also reported by [3] and [2]. Radial variation of solidity and of velocity through the rotor plane should also be representative for studying impact with floating bodies as this would affect the trajectory through the rotor plane affecting blade impact. Tangential velocity at the rotor plane is a function of induced torque for which power coefficient, C_P, and Tip Speed Ratio of the model should be of representative magnitude. However this is typically limited for reduced scale experiments by the maximum lift to drag ratio of a blade section. Here the chord Reynolds number at three-quarter span is typically greater than 100,000 and peak power coefficient is 0.4.

Radial variation of blade geometry was selected using a standard BEM approach assuming steady flow and neglecting blockage. A RANS-BEM method was subsequently employed (based on [20]) for a flume of depth 1.67 times diameter and global blockage of 0.14 to obtain radial variation of blade loads. At a tip speed ratio 4.5 the maximum mean torque predicted per blade was 50 Nm, due to quasi-steady superposition of current and wave. This is equivalent to a point load of 83 N applied at the tip which contrasts with the peak force of over 4 kN measured (Figure 3) for impact with a rubber surface and with negligible dependent on mass of the impacted body. Preliminary tests with a deformable target indicate a significantly lower force, by an order of magnitude, due to impact with a 'soft part', representative of blubber, and it is expected that impact loads would be lower for a target located in water. However, there remains uncertainty concerning scaling of impact loads and the magnitude of the extreme case remains to be quantified and so blade design herein is based on the predicted hydrodynamic load.

B. Structural Analysis

In order to iterate efficiently through successive blade designs, the structural model was based on beam theory rather than three dimensional finite element analysis (FEA). The beam considered is of variable section. It is made of 80 discreet sections of constant span over the blade length (figure 6).

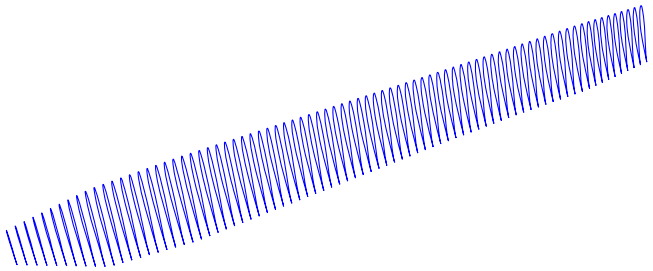

Fig. 6. Discretisation of blade profile into 80 evenly spaced sections.

The moments of inertia of each blade section were computed by two dimensional FEA using the software Abaqus. Figure 7 shows an example of section discretisation.

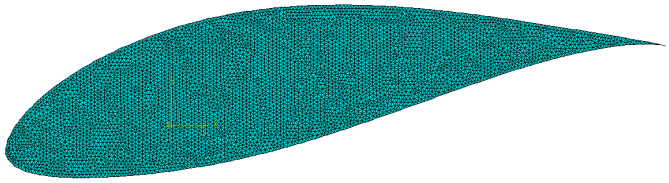

Fig. 7. Discretisation of a two dimensional blade section

Moments of inertia and streamwise and off-axis forces are input into Abaqus again to solve the beam equations yielding the deflection at each section. Abaqus allows Python scripting which made it possible to automate and integrate together the different stages of the structural analysis together with the BEM model coded in Matlab. The overall model computes deflections from blade geometry, blade material properties, free stream velocity and turbine rotational speed.

One of the key structural design choice for the blade was the material they should be made of. Metal and composite were originally considered but the latter was eventually discarded because it could not be fabricated internally. Aluminium was first considered because it is easy to machine. However, the Young modulus of aluminium proved to be too low to keep the tip deflection within the 2% target. In the end 304 stainless steel was chosen. Figure 8 shows blade deflection as a function of radius for aluminium and stainless steel. These results were obtained from the combine BEM and Abaqus beam model described above with a flow total flow velocity of 1.28ms^{-1} (free stream velocity of 1ms^{-1} + wave induced velocity of 0.28ms^{-1}) and a TSR of 5. It can be seen that in the streamwise direction (where the loads are the highest the and blade dimension the thinnest), aluminium is predicted to lead to tip deflection of 15mm which is higher than the 12mm limit.

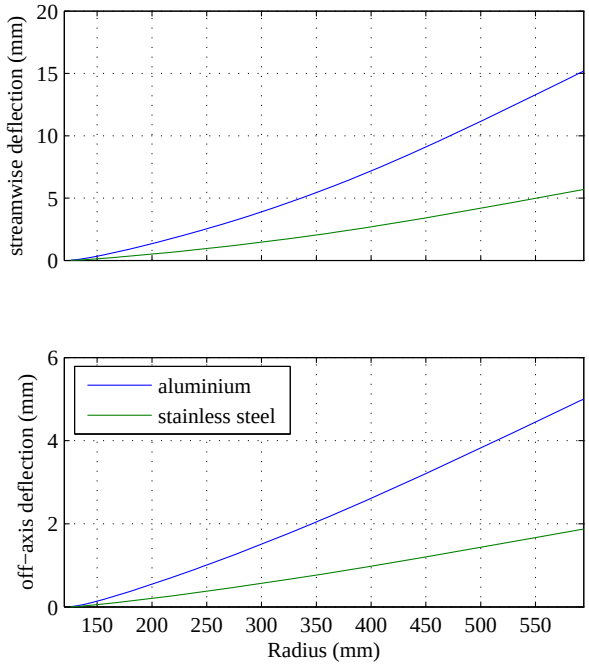

Fig. 8. Streamwise (top) and off-axis (bottom) blade deflection plotted against radius for two blade materials

Once the blade design had been refined using the integrated BEM and beam theory model, a final check of the blade structure integrity and deflection was carried out using three-dimensional FEA with the SolidWorks Simulations software. The loads used as input for that FEA model were derived from the BEM model. Figure 9 shows the blade deflection predicted by the FEA model. For the final blade design, the discrepancy between the beam theory results and the SolidWorks Simulations FEA in terms of combined streamwise and off-axis tip deflection is only of 6%.

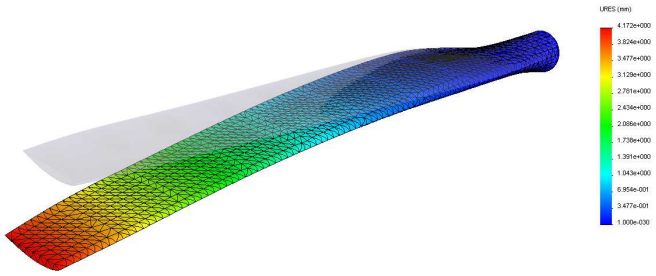

Fig. 9. Blade deflection predicted by FEA

IV. Nacelle design

One of the purposes of testing the turbine model is to use the experimental measurements to validate CFD simulations in which the rotor spins at constant speed.

A. Drivetrain design

A servo motor was selected to resist the current induced torque of the rotor as this type of electrical machine is well suited for speed control. The servo motor will therefore perform most of the time as a brake (rather than a motor), dissipating the power generated into a break resistor.

The main design constrains for the servo motor are its torque capacity and its size. The original aim was to make sure that the nacelle diameter did not exceed 10% of the rotor diameter (i.e. 120mm). However, given the size of the rotor and the fact it is to be tested in extreme conditions, from the BEM computations, the motor should be able to cope with transient torques of 50Nm. An off-the shelf motor with this torque capacity and suitable form factor was not identified. Indeed, most small diameter motors tend to be high speed and low torque. The use of a gearbox was therefore considered to step-up to torque. However, most gearboxes for servo motors are designed to be used driven from the motor side and not the other way round like it is the case when the motor simulates a generator. When used in the direction they are not designed for, gearboxes exhibit significantly lower efficiency but more importantly, the gears on the high torque side of the gearbox experience loads that they are not designed for. The latter problem is particularly severe when the gearbox has two or more stages. It was therefore decided to relax the limitation on the motor diameter so that direct drive could be used. The final motor selected is 145ST4M 500rpm by Alxion and with outer diameter 145mm.

B. Instrumentation

One of the advantages of the fairly large scale of the turbine model is that it provides more space for instrumentation. The model is fitted with a force transducer at the root of each blade to measure the streamwise root bending moment. The flexure of that transducer is a square section beam, two sides of which are fitted with strain gauges. Strictly speaking the strain measured in this manner is affected by both bending moment and shear. However a FEA analysis of the flexure has been carried out with the maximum loads predicted by the RANS-BEM model and it shows that the strain predicted is caused at 96% by bending moment. It is therefore deemed acceptable consider the reading from those transducers as a good indication of the root bending moment. The flexures were strain gauged, waterproofed and calibrated by the company Applied Measurements Ltd.

A torque and thrust transducer is mounted between the hub and the shaft to measure the overall thrust and torque generated by the rotor. This transducer has no rotating part and can be considered as an ‘instrumented extension’ of the shaft. It is waterproof and located ‘upstream’ of the shaft rotary seal so that the friction induced by the seal does not affect the torque measurements. The transducer was custom made by Applied Measurements Ltd. The servo-motor is controlled in speed based on a built-in two-pole resolver. This

outputs angular position of the shaft which is post-processed for rotor speed..

C. Model design overview

Figure 10 shows a section view of the CAD model of the turbine experimental model where the overall arrangement of the different components can be seen. The strain gauge amplifiers of the root bending moment transducers are located in the nose waterproof enclosure. The amplifiers of the torque and thrust transducer are housed inside the transducer itself. The wiring from the nose is passed through torque and thrust transducer and exits, with the wiring for the torque and thrust transducer itself through the shaft which is hollow on its end connected to the transducer. Further aft, the shaft passes through a waterproof rotary seal. The wiring then exits the shaft radially and is connected to a slipring. The motor is located at the back as far away as possible from the shaft and blade transducers and their connected wiring to minimise signal pollution by electromagnetic interference.

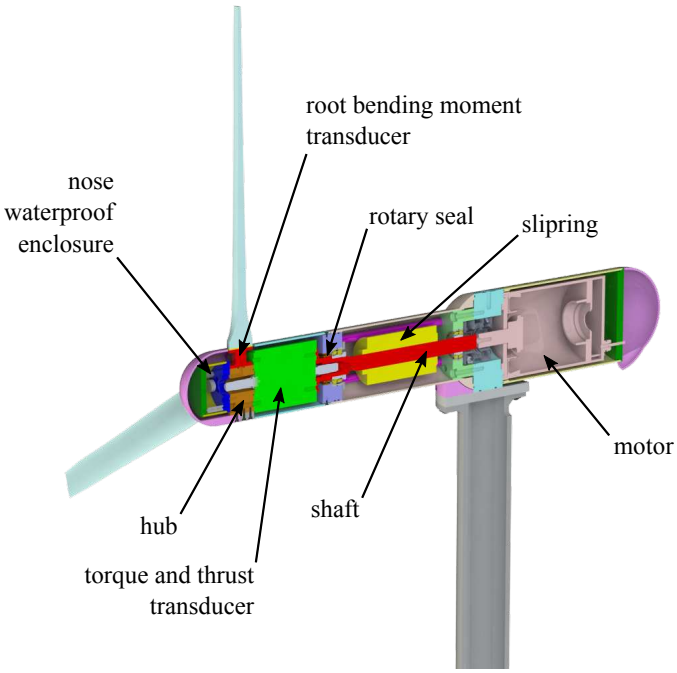

Fig. 10. Section view of the CAD model of the turbine experimental model

V. Summary

Design of tidal stream turbines requires accurate prediction of the loading experienced due to the range of turbulent flows and waves occurring during the operating life and potentially due to impact from floating bodies. An overview is given of the development of a turbine of approximately $1/15^{th}$ scale for investigating such loads. The arrangement of the test has been selected to provide comparison with prior and ongoing experimental and numerical studies at differing scales at particular operating points. Rotor geometry has been selected to minimise tip deflection, for constant speed operation, to allow measurement of shaft torque and blade root bending. The design has been developed considering hydrodynamic loads due to the maximum combination of a steady flow and the depth decay of waves.

To inform turbine and blade design a preliminary assessment of impact loads has been conducted using a range of custom targets which represent the material characteristics of marine animals. Data from these tests indicate that peak instantaneous load due to impact with a rubber coated body may be a factor of fifty greater than the blade load due to mean flow superposed with peak wave velocity as predicted by a standard blade element momentum method. In that context it was considered of limited value to use the same experimental arrangement to investigate these two types of loads. Impact load exhibited negligible dependence on the mass of the object impacted. However, impact load reduces with the stiffness of the object impacted. Preliminary measurements with a target representing the material properties of blubber indicated forces approximately one tenth of those on a rigid target with rubber coating representing the material properties of the harder sections of a marine vertebrate. This suggests impact loads with a deformable body of over three times the mean hydrodynamic load. These may be lower for a body impacted in water but the extreme case may be impact with hard object or part.

Additional experimental data concerning impact loading will be presented at the conference. Findings from tank tests of the turbine will also be presented including the variation of rotor and blade loading with onset turbulence intensity, and onset turbulence with waves. The focus is on the variation of loading and peak loading in these flow conditions. Comparison will be drawn to prior experimental studies at reduced scale.

Acknowledgements

This study was supported by funding provided by the EPSRC grant X-MED (EP/J010235/1).

References

[1] M. Togneri, I. Masters, and J. Orme, “Incorporating Turbulent Inflow Conditions in a Blade Element Momentum Model of Tidal Stream Turbines,” in *Proceedings of the 21^{st} International Offshore and Polar Engineering Conference*, Mauii, Hawaii, June 2011.

[2] S. Way and W. Collier, “Full-scale validation study of a numerical tool for the prediction of the loading and hydrodynamic performance of axial flow tidal turbines,” in *Proceedings of the 10^{th} European Wave and Tidal Energy Conference*, Aalborg, Denmark, September 2013.

[3] P. Mycek, B. Gaurier, G. Germain, G. Pinon, and E. Rivoalen, “Experimental study of the turbulence intensity effects on marine current turbines behaviour. Part II: Two interacting turbines,” *Renewable Energy*, vol. 66, pp. 727–746, 2014.

[4] L. Chamorro, C. Hill, S. Morton, C. Ellis, R. Arndt, and F. Sotiropoulos, “On the interaction between a turbulent open channel flow and an axial-flow turbine,” *Journal of Fluid Mechanics*, vol. 716, pp. 658–670, 2013.

[5] I. Afgan, J. McNaughton, S. Rolfo, D. Apsley, T. Stallard, and P. Stansby, “Turbulent flow and loading on a tidal stream turbine by LES and RANS,” *International Journal of Heat and Fluid Flow*, vol. 43, pp. 96–108, 2013.

[6] N. Barltrop, K. Varyani, A. Grant, D. Clelland, and X. Pham, "Investigation into wave-current interactions in marine current turbines," *Proc. IMechE Part A: J. Power and Energy*, vol. 221, pp. 233–242, 2007.

[7] P. Galloway, L. Myers, and A. Bahaj, "Quantifying wave and yaw effects on a scale tidal stream turbine," *Renewable Energy*, vol. 63, pp. 297–307, 2014.

[8] B. Gaurier, P. Davies, A. Deuff, and G.Germain, "Flume tank characterisation of marine current turbine blade behaviour under current and wave loading," *Renewable Energy*, vol. 59, pp. 1–12, 2013.

[9] E. Fernandez-Rodriguez, T. Stallard, and P. Stansby, "Experimental study of extreme thrust on a tidal stream turbine in turbulent flow and with opposing waves," *Journal of Fluids and Structures*, vol. 51, pp. 354–361, 2014.

[10] T. Carlson, B. Watson, J. Elster, A. Copping, M. Jones, M. Watkins, R. Jepsen, and K. Metzinger, "Assessment of Strike of Adult Killer Whales by an OpenHydro Tidal Turbine Blade," US DOE contract DE-AC05-76RL01830 report PNNL-21177 Appendix K, Tech. Rep., February 2012.

[11] B. Wilson and S. Benjamins, "Personal communication," in *Scottish Association of Marine Sciences (SAMS)*, 2013.

[12] J. Whelan and T. Stallard, "Arguments for modifying the geometry of a scale model rotor," in *Proceedings of the* 9^{th} *European Wave and Tidal Energy Conference*, Southampton, UK, September 2011.

[13] T. Stallard, T. Feng, and P. Stansby, "Experimental study of the mean wake of a tidal stream rotor in a shallow turbulent flow." *Journal of Fluids and Structures*, vol. DOI: 10.1016/j.jfluidstructs.2014.10.017, 2014.

[14] C. Fleming, S. McIntosh, and R. Willden, "Tidal turbine performance in sheared flow." in *Proceedings of the* 10^{th} *European Wave and Tidal Energy Conference*, Aalborg, Denmark, September 2013.

[15] J. McNaughton, S. Rolfo, D. Apsley, T. Stallard, and P. Stansby, "Comparison of three turbulence models for RANS modeling of Tidal Stream Turbine loading and wake." in *Proceedings of the* 1^{st} *Asian Wave and Tidal Energy Conference*, October 2013.

[16] S. M. Longshaw, P. K. Stansby, and B. D. Rogers, "Whale To Turbine Impact Using The GPU Based SPH-LSM Method," in 9^{th} *International Smoothed Particle Hydrodynamics European Research Interest Community (SPHERIC) Workshop*, Paris, France, 2014.

[17] J. Newman, *Marine Hydrodynamics*. The MIT Press, 1977.

[18] M. O. L. Hansen, *Aerodynamics of Wind Turbines*, 2nd ed. Earthscan, 2008.

[19] T. Sarpkaya and M. Isaacson, *Mechanics of Wave Forces on Offshore Structures*. Van Nostrand Reinhold, 1981.

[20] R. Malki, A. J. Williams, T. N. Croft, M. Togneri, and I. Masters., "A coupled Blade Element Momentum-Computational Fluid Dynamics model for evaluating tidal stream turbine performance," *Applied Mathematical Modelling*, vol. 37, pp. 3006–3020, 2013.